HAIT Journal of Science and Engineering B, Volume x, Issue x, pp. xxx-xxx

The head-on collision of normal shock waves with a concrete supported plate

Gedalia Mazor[1], Dmitry Nemirovsky[2,*], and Uri Tzadka[3]

[1] *Mechanical Engineering Department*
[2] *Physics Department*
[3] *Civil Engineering Department*
Sami Shamoon College of Engineering, Beer-Sheva 84100, Israel
[*] *Corresponding author: demitryi@bgu.ac.il*
Received 12 November 2007, accepted 3 January 2008

Abstract

The head-on reflection of normal shock waves from a concrete-supported plate was investigated numerically. The computer simulation of the collision process, based on a code developed by us, utilizes the mass, momentum and energy conservation equations, supplemented by relations for the velocity, compressive strain and equation of state. The differential equations and conservations laws are used for the shock wave propagation treatment using the finite difference approach for the second order space-time equations. In order to eliminate the singularity in vicinity of the shock wave front, the artificial viscosity approach has been used. Results obtained by the simulation include, among others, the time and space dependence of the pressure and the velocity both in the gaseous phase and solid medium. Furthermore, the relationship between the characteristic concrete compressive strength and its ability to sustain shock wave dynamic loading, important for the concrete structures design, has been obtained numerically.

Keywords: Shock wave propagation, Dynamic loading, Concrete plate
PACS: 46.15.-x, 46.70.De, 47.40.Nm

1 Introduction

The process of normal shock-waves collision with a concrete wall is of considerable importance from both the theoretical and engineering points of view. The ability to predict the overall picture of the stress field for a concrete wall of prescribed physical properties, exposed to shock waves, is important for designing the walls. The numerical simulation of shock-wave collision, reflection and transmission may also contribute to the investigation of concrete wall behavior in the compressed state. From an industrial standpoint it is necessary to estimate the minimal width and mechanical properties of the concrete wall that can withstand shock-waves of given intensity. Such information is vital for designing protective shielding for people, as well as civil and military structures. The numerical scheme and the computer code for the shock-wave propagation and interaction problem have been developed in the context of the present investigation.

Normal shock wave interaction with solid walls can be divided into two main categories: head-on reflection from rigid solid walls and flexible solid walls. The reflection from the rigid wall was first investigated by [1] and [2]. [3], [4] and [5] have extended the topic by permitting the rigid solid wall to move. [6] and [7] examined the head-on reflection from a rigid solid porous wall. Head-on reflection from a stationary linear elastic solid was explored by [8] and [9] that took into account the possibility of stationary solid wall deformation. The head-on reflection from a stationary porous flexible wall has been studied by [10], [11] and [12]. A solid plate, supported by a deformable damping system, interacting with the head-on shock-wave, was described by [13]. The subject was appended significantly by Mazor and Ben-Dor [14-18] who examined, for the first time, both experimentally and theoretically, the normal head-on shock-wave collision with elastic nonlinear materials such as rubber and sponge, subjected to strong deformations. In the theoretic field, the pessure field equations for the gaseous domain and the stress field equations for the solid domain have been developed and solved numerically. In addition to the above-mentioned contribution, the analytical expression for the shock-wave emergence localization in the solid phase has been obtained.

Our investigation, dedicated to the study of the reflected shock wave in the gaseous phase and the shock wave propagation inside the concrete of a given stress-strain relation, has a twofold purpose:

1. The better understanding of the shock wave interaction with a concrete rod.

2. The developing and testing of the numerical simulation code, devoted to the study of the shock wave propagation in concrete medium.

This problem is essentially one-dimensional from the physical standpoint; hence we decided to choose the 1D numerical solution that fits the problem under consideration. We would like to mention that all papers, referenced in this section, utilize the same 1D approach.

Some further results refer to the concrete specimen behavior (velocity and stress distributions) during the shock wave propagation.

2 Theoretical background

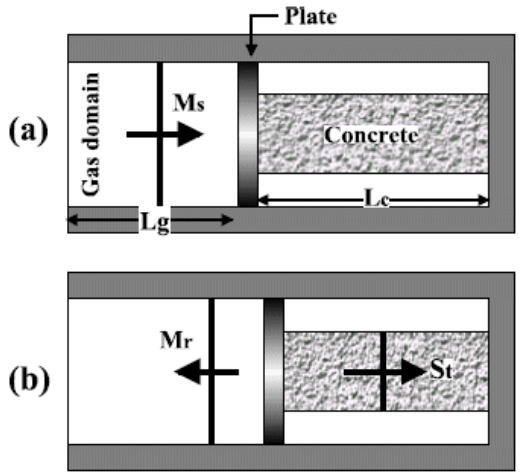

Figure 1: Schematic illustration of the problem under consideration: a) prior to the head on collision; b) immediately after the head on collision.

The simulated system we are going to deal with is represented schematically in Fig. 1. A concrete rod (of initial length L_c and cross-sectional area A_c), covered by a rigid flat plate (having mass M_d and cross-section A_g),is supported at its rear by the end wall of the shock tube. A shock wave of Mach number M_s, that propagates in a gas, hits the plate. As a result of the sudden pressure increase, the flat plate accelerates and compresses

the concrete rod that supports it. Subsequently, the reflected shock wave of Mach number M_r is reflected back to the gas domain and a transmitted shock wave S_t is propagated into the concrete specimen. The incident shock-wave Mach number is defined as $M_s = V_s/a_1$, where V_s is a shock-wave velocity and a_1 is the sound speed.

As an expansion of the specimen is limited only at the rear end (along the x-axis) and there are no constraints along the y- and z-axes (towards the shock tube walls), the only uni-axial stress compression ($\sigma_y = \sigma_z = 0$ and $\epsilon_y = \epsilon_z \neq 0$, where ϵ_i and σ_i are the strain and the stress in the i-th direction respectively) should be taken into account.

The simulation model of the interaction process is based on the following assumptions:

1. The model is nonstationary and one-dimensional.

2. The gas is an ideal fluid, i.e., inviscid ($\mu = 0$) and thermally non-conductive ($k = 0$).

3. The gas behaves as a perfect gas, i.e., its equation of state is $P = \rho RT$ and its internal energy, e, is given by $e = C_v T$, where P, ρ, and T are the gas pressure, density, and temperature, respectively, C_v is its specific heat capacity at a constant volume and R is its specific gas constant.

4. The gravitational forces are neglected in both the gaseous and the solid phases.

5. The compressed material is a uniform solid phase in which the mechanical properties are related to its structure and to the material properties.

6. The friction forces acting on the external surfaces of the concrete rod are neglected.

7. The stresses, which develop in the concrete rod, are uniformly distributed inside any cross-sectional area and normal to the cross-section. Therefore, the cross-sectional area remains planar throughout the deformation stages of the concrete rod.

8. The concrete rod does not buckle but is only compressed.

3 The governing equations

The governing equations, based on the above assumptions, are developed using a Lagrangian approach (for details see [15]).

For the gaseous domain the governing equations are:
mass conservation:

$$\frac{\partial}{\partial t}\Big(\rho_g(h_g,t)\frac{\partial x(h_g,t)}{\partial h_g}\Big)=0, \tag{1}$$

gas velocity:

$$U_g(h_g,t)=\frac{\partial x(h_g,t)}{\partial t}, \tag{2}$$

linear momentum conservation:

$$\frac{\partial U_g(h_g,t)}{\partial t}=-A_g\frac{\partial P(h_g,t)}{\partial h_g} \tag{3}$$

energy conservation:

$$\frac{\partial e(h_g,t)}{\partial t}=-P(h_g,t)\frac{\partial V_g(h_g,t)}{\partial t} \tag{4}$$

where $e(h_g,t)=C_vT(h_g,t)$ is the internal energy
and the V_g, the specific volume ($V_g=1/\rho_g$).

The equation of state:

$$P(h_g,t)=\frac{RT(h_g,t)}{V_g(h_g,t)}. \tag{5}$$

When the lagrangian approach is utilized, every mass element may be recognized by a number h which indicates its location in the $x-t$-plane. Usually, this number identifies the mass element position at some time. The definition of h is based on the mass conservartion law. Let us consider a flow streaming along a duct of a constant cross-section area. The flow direction, therefore, may be chosen as the x-axis direction. When the value $h=0$ is assigned to some reference segment in the duct, h simply expresses the mass confined in the duct between the section h and the segment of reference:

$$h=\int_{x(0,t)}^{x(h,t)}\rho A dx$$

In the equations (1 - 5) h_g is the Lagrangian variable for the gaseous phase:

$$h_g = \int_{x(0,t)}^{x(h_g,t)} \rho_g A_g dx$$

For the concrete region the governing equations are:
mass conservation:

$$\frac{\partial}{\partial t}\Big(\rho_c(h_c,t)\frac{\partial S(h_c,t)}{\partial h_c}\Big) = 0 \tag{6}$$

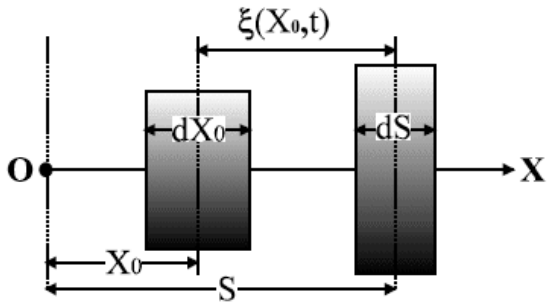

Figure 2: A diagrammatic sketch of a mass element prior to its deformation and thereafter.

To define a particle velocity inside the concrete let us consider a mass element dm which at $t = 0$ was at $x = X_0$ and had a width dX_0 (see Fig. 2). As a result of the concrete deformation , this mass element moves to a new position, S, and its width is changed to dS. It is evident from Fig.2 that $S = X_0 + \xi$ where ξ is the magnitude of the displacement along the X-axis. The concrete cell velocity may therefore be defined as,

$$U_c(h_c,t) = \frac{\partial S(h_c,t)}{\partial t} \qquad \text{or} \qquad U_c(h_c,t) = \frac{\partial \xi(h_c,t)}{\partial t} \tag{7}$$

The extension ratio in the x-direction, λ_x, expresses the ratio between the mass elements widths after and before deformation:

$$\lambda_x(h_x,t) = \frac{\partial S(h_c,t)}{\partial X_0}$$

With the addition of $\frac{\partial S(h_c,t)}{\partial X_0} = \frac{\partial S(h_c,t)}{\partial h_c}\frac{\partial h_c}{\partial X_0}$

and the definition of the Lagrangian variable for the concrete specimen, h_c, i.e.,

$$h_c = \int_{S(0,t)}^{S(h_c,t)} \rho_c A_c dS$$

expression for the λ_x may be rewritten as:

$$\lambda_x(h_c, t) = \rho_c^0 A_c \frac{\partial S(h_c, t)}{\partial h_c}$$

where the superscript 0 indicates pre-deformation values. For a material under compressive loads $0 < \lambda_x < 1$ and for a material under tensile loads $\lambda_x > 1$. When the material is load free (i.e., stress free conditions) $\lambda_x = 1$. The strain in the x-direction can be simply obtained from the definition $\epsilon_x = \lambda_x - 1$, i.e.,

$$\epsilon_x(h_c, t) = \rho_c^0 A_c \frac{\partial S(h_c, t)}{\partial h_c} - 1 \tag{8}$$

For a mass element dm where $dm = \rho_c A dS = \rho_c^0 A dX_0$, Newton's second law implies

$$\frac{\partial}{\partial t}(dm U_c) = -\frac{\partial F_x}{\partial X_0} dX_0$$

where F_x is the normal force acting on a given cross section at time t. Substituting (7) with the definition of the mass element into the above expression results in,

$$\rho_c^0 A_c \frac{\partial^2 \xi(h_c, t)}{\partial t^2} = -\frac{\partial F_x(f_c, t)}{\partial X_0}$$

The above expression represents the conservation of momentum of the concrete cell. By introducing the stress in the x-direction,

$$\sigma_x(h_c, t) = \frac{F_x(f_c, t)}{A_c}$$

the above expression becomes

$$\frac{\partial^2 \xi(h_c, t)}{\partial t^2} = -\frac{1}{\rho_c^0} \frac{\partial \sigma_x(h_c, t)}{\partial X_0}$$

However, since

$$\frac{\partial \sigma_x(h_c, t)}{\partial X_0} = \frac{\partial \sigma_x(h_c, t)}{\partial h_c} \frac{\partial h_c}{\partial X_0} = \frac{\partial \sigma_x(h_c, t)}{\partial h_c} \rho_c^0 A_c$$

one obtains

$$\frac{\partial^2 \xi(h_c,t)}{\partial t^2} = -A_c \frac{\partial \sigma_x(h_c,t)}{\partial h_c}$$

But as shown in Fig. 2, $S = X_0 + \xi$, hence the equation of motion of the concrete is,

$$\begin{aligned} \frac{\partial^2 S(h_c,t)}{\partial t^2} &= -A_c \frac{\partial \sigma_x(h_c,t)}{\partial h_c} \qquad \text{or} \\ \frac{\partial U_c(h_c,t)}{\partial t} &= -A_c \frac{\partial \sigma_x(h_c,t)}{\partial h_c} \end{aligned} \tag{9}$$

Equations (1) to (9) comprise a set of nine governing equations with ten independent variables, namely, ρ_g - the density in the gaseous phase, P - the pressure in the gaseous phase, T - the temperature in the gaseous phase, U_g - the velocity of the particles m the gaseous phase x - the displacement in the gaseous phase, ρ_c - the density in the concrete domain, σ_x - the normal stress (in the x-direction) in the concrete region, U_c - the velocity of the concrete particles, ϵ_x - the strain (in the x-direction) in the concrete and, S - the displacement in the concrete.

Consequently, in order to have a closed set of equations, which, in principle, could be solved, there is a need for an additional equation. The additional equation is the constitutive relation which is known more commonly as the stress-strain relation, i.e.,

$$\sigma_x = \sigma_x(\epsilon_x)$$

This equation dictates how materials, including concretes, will respond to a sudden load imposed by a head-on colliding shock wave.

The stress-strain relation used in the simulation is derived from the Modified Scott Model ([19]) based on the experimental results for high stress concrete ([20, 21]) in a dynamic load. This model is applicable to the concrete strength up to 100 MPa. The model is governed by the following equations:

$$|\sigma(\epsilon)| = \begin{cases} f_c \left[2\frac{|\epsilon|}{|\epsilon_0|} - \left(\frac{\epsilon}{\epsilon_0}\right)^2 \right] & \text{for } |\epsilon| \le |\epsilon_0| \\ \\ f_c \left[1 - \frac{0.15}{|\epsilon_1 - \epsilon_0|} |\epsilon - \epsilon_0| \right] & \text{for } |\epsilon_0| < |\epsilon| < |\epsilon_1| \end{cases} \tag{10}$$

(where f_c is a compressive strength) and illustrated in Fig.3.

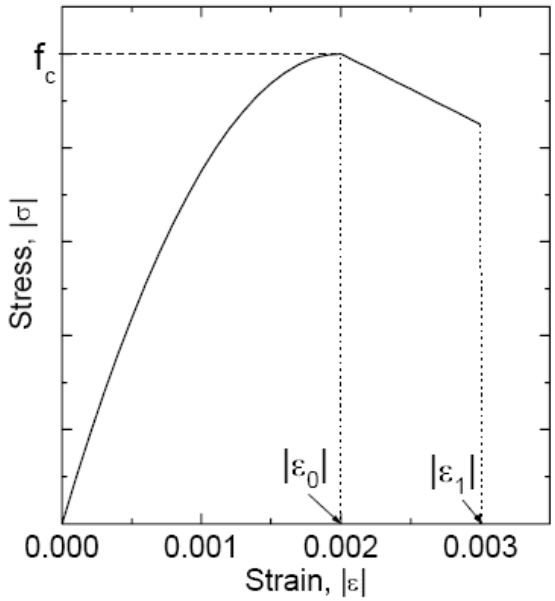

Figure 3: Stress-strain curve that governs the Modified Scott Model for a concrete subjected to a compressive dynamic load.

The descending branch of the stress-strain curve of concrete is a region where a disruption of concrete begins. The failure is caused by the development of splitting cracks in the direction of the applied load and due to the development of an inclined shear band. When the developed stress in some region of the simulated specimen exceeds f_c and ϵ falls into the descending region of the strain-stress curve ($|\epsilon_0| < |\epsilon| < |\epsilon_1|$), we assume the failure of the rod to sustain the loading.

The above listed set of ten governing equations must be solved simultaneously for the following boundary conditions,

$$\begin{aligned} U_g(h_g = H_g, t) &= U_c(h_c = 0, t) \\ U_c(h_c = H_c, t) &= 0. \end{aligned} \tag{11}$$

The first condition implies that the velocities of the gaseous phase and the concrete at the interface between them are identical, and the second one implies that the rear face of the concrete rod which is supported by the shock tube end-wall, see Fig. 1, has a zero velocity at all times. The value of

$U_c(h_c = 0, t)$ which appears in the right hand side of (11) can be evaluated by the following equation,

$$\frac{\partial U_c(h_c = 0, t)}{\partial t} = \frac{2A}{\Delta h_g + \Delta h_c}(P_g(h_g = H_g, t) - |\sigma_x(h_c = 0, t)|) \tag{12}$$

4 The numerical scheme

Equations (1) to (9) form a set of partial differential equations that cannot be solved analytically. Hence, a numerical scheme, capable of handling flow discontinuites has been developed. In order to eliminate the singularity in proximity of the shock wave front, the artificial viscosity approach has been applied. The idea of overcoming the spurious oscillation problem in the hydrodynamic equations by introducing an artificial viscosity to damp the amplitude was proposed by [22] in the context of the Euler equations. To do this we introduce an artificial dissipative term whose form and strength are such that the shock transition becomes smooth, extending over a small number of intervals of the space variable. In their original work, Von Neumann and Richtmyer proposed the following expression for the viscosity term (for the gas domain):

$$q_g = \begin{cases} \frac{(C_g \Delta h_g)^2}{V_g(h_g,t)} \left(\frac{\partial V_g(h_g,t)}{\partial t} \right)^2 & , \quad \frac{\partial V_g(h_g,t)}{\partial t} < 0 \\ \\ 0 & , \quad \frac{\partial V_g(h_g,t)}{\partial t} \geq 0 \end{cases} \tag{13}$$

where C_g is a nondimensional constant which controls the simulated shock wave thickness in the gas domain. The commonly used values of C_g lie in the range between 1.5 and 2, spreading the shock over 3-5 intervals of Δh_g. From (13) one can see that the artificial viscosity term becomes significant only in the vicinity of the shock wave front. This term should be added to the linear momentum conservation (3) and state (5) equations, yielding

$$\frac{\partial U_g(h_g, t)}{\partial t} = -A_g \frac{\partial}{\partial h_g}(P(h_g, t) + q_g(h_g, t)) \tag{14}$$

and

$$R \frac{\partial T(h_g, t)}{\partial t} = -(P(h_g, t) + q_g(h_g, t)) \frac{\partial V_g(h_g, t)}{\partial t} \tag{15}$$

In the same way the linear momentum conservation equation (9) may be appended by the artificial viscosity term:

$$\frac{\partial U(h_c,t)}{\partial t} = -A_c \frac{\partial}{\partial h_c}(|\sigma_x(h_c,t)| + q_c(h_c,t)) \tag{16}$$

where the artificial viscous pressure term for the concrete is:

$$q_c = \begin{cases} \frac{(C_c \Delta h_c)^2}{\lambda_x(h_c,t)} \left(\frac{\partial \lambda_x(h_c,t)}{\partial t} \right)^2 & , \quad \frac{\partial \lambda_x(h_c,t)}{\partial t} < 0 \\ \\ 0 & , \quad \frac{\partial \lambda_x(h_c,t)}{\partial t} \geq 0 \end{cases} \tag{17}$$

where C_c is similar to C_g in (13) and responsible for the simulated shock wave width in the concrete sample. Values of C_c also fall into the interval 1.5-2, spreading the wave to 3-5 intervals of Δh_c.

The choice of the C is inspired by the considerations of stability and smoothness of the numerical solution. It was found numerically that the value C=1.8 provides the optimal stability of the solution both in the gas and the solid (concrete) continuum. The same value of C was found elsewhere ([15]) for the normal shock wave interaction with a rubber rod.

The array of nine equations after the artificial viscosity term modification becomes a set of finite difference second order space-time equations.

5 Results and Discussion

5.1 Initial conditions

The simulated system consiss of the three main parts:

1. The space filled with air at 1 atm pressure (prior to the beginning of the shock-wave propagation). The initial length of this space is L_0 and the base area is A_g.

2. The flat plate of mass M_d (negligibly small comparing to the mass of the concrete specimen) and area A_g, covering the main concrete sample.

3. The concrete rod of initial (uncompressed) length L_c, and base area A_c, supported at the rear by the rigid wall.

The present simulation has been performed for the following set of parameters in order to investigate the concrete sample behaviour after the

head-on shock wave collision: L_0= 9 m , A_g/A_c=2, L_c= 1 m, the concrete sample initial density ρ=2400 kg/m^3, f_c= 40 MN/m^2, ϵ_0=0.002, ϵ_1=0.003, initial temperature T=300 K. The shock wave, generated in the gaseous region of the shock-wave facility has a Mach number M_s=3.5

5.2 Compression waves to a shock wave transformation conditions inside a concrete rod

When the incident shock-wave exhibits a head-on collision with the front edge of a concrete rod, a compression wave C_t is transmitted into the concrete region. [23] showed that each pulse in the wave propagates at a velocity, c given by,

$$c = U_c + \lambda_x c_0$$

where c_0, the shift rate of the disturbance, is determined by [1]

$$c_o = \sqrt{\frac{1}{\rho_c^0}\frac{\partial \sigma_x}{\partial \lambda_x}} \tag{18}$$

where c_0 isn't a local sound speed in the concrete. [1] have shown that the proper expression for the local sound speed is given by

$$a = c_0 \frac{\rho_c^0}{\rho_c}.$$

Therefore, the local sound speed is equal to c_0 only in uncompressible materials. It can be seen from (18) that the stress-strain relation of the concrete determines whether or not compression waves, generated at early stage in the compressed concrete rod, propagate slower or faster than those generated at later times. When pulses, produced at early time of the compression process, propagate at a smaller velocity than those produced later, the formation of a shock wave in the rod is forthcoming. [23] showed that the condition for the compression waves, C_t, to converge to a shock wave, S_t, depends on the stress-strain relation of the solid and must fulfill the following two requirements:

1. $\partial\sigma/\partial\lambda > 0$ (Rise in distortion causes rise in stress).

2. $(\partial\sigma/\partial\lambda)_2 > (\partial\sigma/\partial\lambda)_1$ for $\lambda_2 < \lambda_1$ (Rise in distortion causes rise in $(\partial\sigma/\partial\lambda)$.

It is important to note that the above-mentioned transformation conditions are fulfilled for the material under consideration. Therefore, in the present case, a transmitted shock wave, S_t, propagates through the concrete rod as shown in Fig.1(b).

5.3 Simulation results

The pressure distribution in the gaseous domain just after the shock wave initialization (t=0.33 msec, solid line) and following the head-on reflection from the plate (t=3.61 msec, dot line) is depicted in the Fig. 4. One can easily see two distinctive pressure jumps: behind the falling wave front ,M_s (from the atmosferic pressure until 15.2 atm), and in the rear of the reflected wave front ,M_r(untill 80.0 atm), see also Fig. 1.

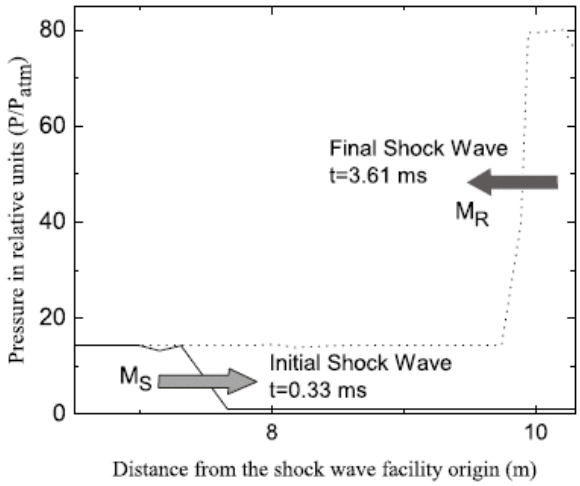

Figure 4: The gas pressure distribution in the gaseous domain of the shock wave facility before and after the head-on collision with concrete supported flat plate.

The transmitted shock wave, S_t (see Fig. 5a), created by the shock wave collision, is propagating through the concrete sample towards the rear wall of the shock-wave tube (region (I)), raising the stress behind the wave front (region (II)). Following the reflection from the tube end, the reflected shock wave, S_r (Fig. 5b) returns back (to region (III)), raising the stress again.

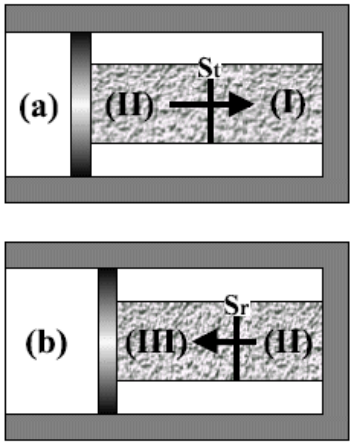

Figure 5: A sketchy illustration of the reflection of the shock wave travelling through a concrete rod: **a** prior to the reflection from the back wall of the shock tube; **b** after the reflection.

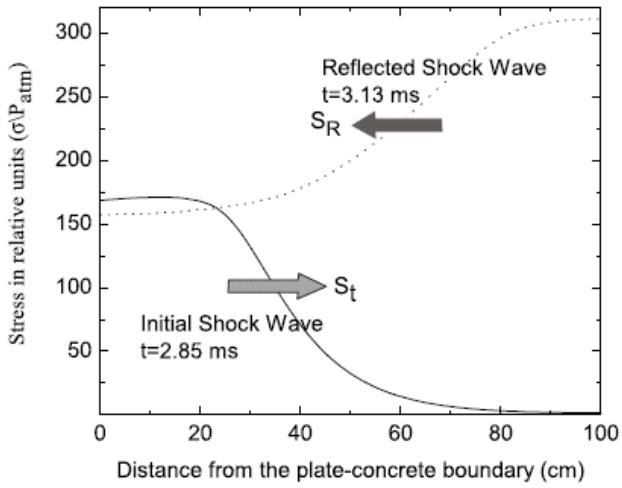

Figure 6: The stress distribution inside the concrete rod illustrating the shock wave propagation before and after reflection from the back wall of the facility.

This process is illustrated quantitatively in Fig. 6. The transmitted shock wave prior to collision (solid line) with the end wall (t=2.85 msec) elevating stress behind the front until 17 MPa approximately. Just after the reflection of this shock wave (dot line) from the rear wall (t=3.13 msec) stress builds up again, achieving the value of 31 MPa. It must be underscored, that both the stress values in the rod (17 MPa and 31 MPa) are smaller than $f_c = 40$ MPa and therefore the concrete rod sustains the shock wave dynamic loading in this case ($M_s = 3.5$).

It would be interesting to examine the velocity of the flat plate as a function of time (see Fig. 7). After the head-on collision of the incident shock wave the plate accelerates to the end wall direction, reaching, after the short time, a constant velocity of 175 cm/s. The reflected shock wave, S_r, causes the plate to change its traveling direction to the opposite direction and to attain a constant velocity of -175 cm/s while moving leftwards (negative velocity). A rarefaction wave, transmitted later to the gaseous domain, changes the plate movement direction again.

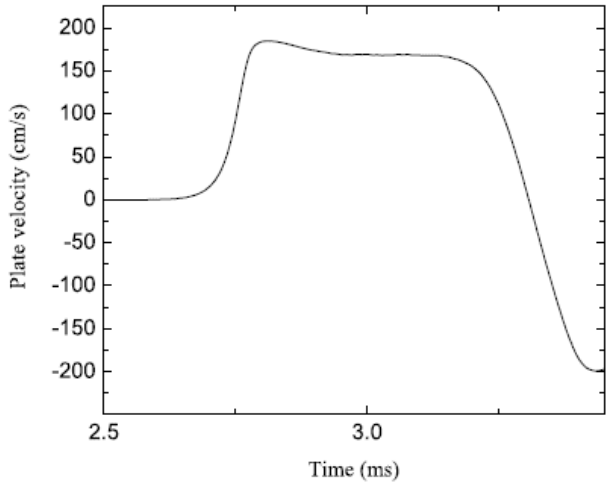

Figure 7: The flat plate velocity as a function of time.

The variations in the gas pressure, acting on the flat plate and depicted in Fig. 8 are almost identical to the case of shock wave collision with a rigid wall ([15]).

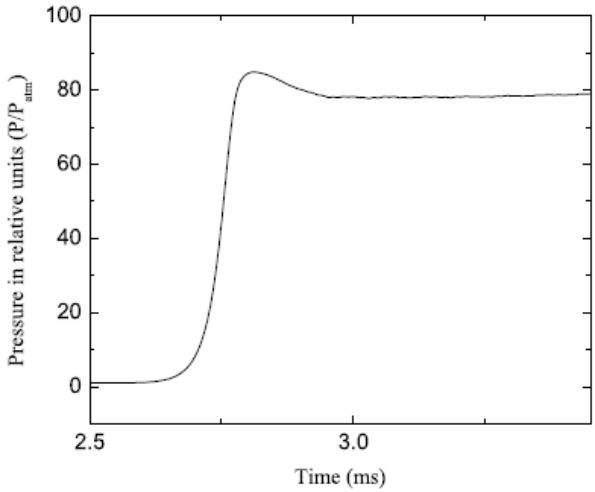

Figure 8: The gas pressure acting on the front of the flat plate as a function of time.

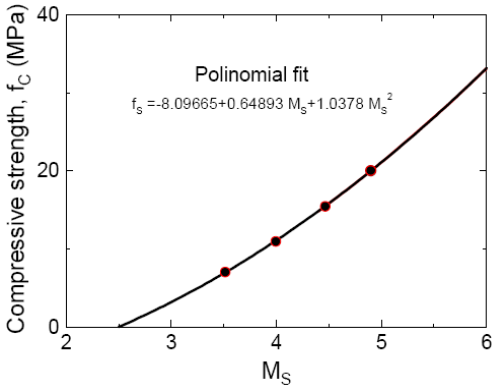

Figure 9: Dependance of the characteristic concrete compressive strength, f_c, on the Mach number, M_s, of the shock wave that causes the concrete specimen destruction.

In addition to the foregoing simulation results, it should be particulary emphasized, that the developed numerical scheme is dedicated mainly to an exploration of dependence of the concrete compressive strength, f_c, on its ability to sustain the dynamic pressure loading applied by the shock-wave

of a given Mach number, M_s. The simulation results are shown in the Fig. 9. Each calculated point represents the smallest compressive strength of the concrete specimen needed to sustain the collision with the shock-wave of given M_s. In order to simulate real collision conditions for the blast wave, we took the ratio $A_g/A_c = 1$. Polynomial fit shows that the relationship between the minimal required compressive strength, f_c and M_s may be interpolated by a simple parabolic function.

6 Final remarks and conclusions

1. Numerical investigations of the interaction of the normal shock waves with a concrete supported plate have been conducted.

2. The dependence of the characteristic concrete compressive strength, f_c, on the Mach number, M_s, of the shock wave that causes the concrete specimen destruction, was found numerically.

3. The next part of our research will be dedicated to the study of shock wave interactions with concrete, shielded by different materials (like aluminium honeycombs). Such exploration will be beneficial in protective shielding design for people, and for civil and military structures.

References

[1] R. Courant and K.O. Friedrichs, *Supersonic Flow and Chock Waves*, (Interscience, New York, 1948).

[2] I.I. Glass and J.G. Hall, *Handbook on Supersonic Aerodinamics,* Navord Rept. 1488, Vol. **6** (Bureau of Naval Weapons, Wasington D.C., 1959).

[3] R.A. Alpher and R.J. Rubin, *Normal reflection of shock waves from moving boundaries*, J. Appl. Phys. **25**, 394 (1954).

[4] R.F. Meyer, *Impact of shock waves on movable wall*, J. Fluid Mech. **3**, 309 (1957).

[5] E. Wlodarczyk, *Shock wave reflection from a plane partition moving in gas*, J. Tech. Phys. **21**, 505 (1980).

[6] G.S. Beavers and R.K. Matta, *Reflection of weak shock waves from permeable materials*, AIAA Journal **10**, 959 (1972).

[7] J.F. Clarke, *Regular reflection of a weak shock wave from a rigid porous wall*, Quart. J. Mech. Appl. Math. **37**, 87 (1984).

[8] D.C. Pack, *Reflection and transmission of shock waves*, Phil. Mag. **2**, 182 (1957).

[9] R. Monti, *Nonnal shock-wave reflection on deformable solid walls*, Mechanica **5**, 285 (1970).

[10] F.H. Wienfield and D.A. Hill, *Preliminary results on the physical properties of aqueous foams and their attenuating characteristics*, DRES, TN-389 (1977).

[11] A.A. Borisov, B.E. Gel'fand, V.M. Kudinov, B.I. Palamorchuk, V.V. Stepanov, E.I. Timofeev, and S.V. Khomik, *Shock waves in water foams*, Acta Astronaut. **5**, 1027 (1978).

[12] B.E. Gel'fand, A.V. Gubanov, and E.I. Timofeev, Fluid Dyn. **18**, 561 (1983).

[13] E. Wlodarczyk, *Stationary shock wave reflection from a solid partition by deformable damping systems*, J. Tech. Phys. **22**, 201 (1981).

[14] G. Mazor, *The influence of surface properties on the head on reflection of shock waves*, Ph.D. Thesis, Dept of Mech. Eng., Ben-Gurion University of the Negev, Beer Sheva, Israel (in Hebrew), 1989.

[15] G. Mazor, O. Igra, G. Ben-Dor, M. Mond, and H. Reichenbach, *Head-on collision of normal shock waves with a rubber supported rod*, Proc. Roy. Soc. Lond., Trans. Roy. Soc. Lond., Ser. A338, 237 (1992).

[16] G. Ben-Dor, G. Mazor, M. Mond, O. Igra, W. Heilig, and H. Reichenbach, *The head-on reflection of a planar shock wave from a rubber wall: The uni-axial strain case*, AIAA Journal **31**, 2184 (1993).

[17] G. Mazor, G. Ben-Dor, O. Igra, and S. Sorek, *Shock wave interaction with cellular materials. I. Analytical investigation and governing equations*, Shock Waves **3**, 159 (1994).

[18] G. Ben-Dor, G. Mazor, G. Cederbaum, and O. Igra, *Well-tailored compressive stress-strain relations for elastomeric foams*, J. Mater. Sci. **31**, 1107 (1996).

[19] T. Ngo, P. Mendis, D. Teo, and G. Kusuma, *Behavior of high-strength concrete columns subjected to blast loading*, Proc. Int. Conf. on Advances in Structures (ASSCCA03), p. 1057, Sydney, 2003.

[20] G. Gary, *Essais à grande vitesse sur béton. Problèmes spécifiques*, Tech. Rep. GRECO, Paris (in French) (1990).

[21] D. Grote, S. Park, and M. Zhou, *Well-tailored compressive stress-strain relations for elastomeric foams*, Int. J. Impact. Eng. **25**, 869 (2001).

[22] J. Von Neumann and F.D. Richtmyer, *A method for the numerical calculation of hydrodynamic shocks*, J. Appl. Phys. **21**, 232 (1950).

[23] J.L. Nowinski, *On the propagation of finite disturbances in bars of rubberlike materials*, J. Eng. Industry **87**, 523 (1965).